J. Fluid Mech. (1996), *vol.* 316, *pp.* 197–221

Gravity granular flows of slightly frictional particles down an inclined bumpy chute

By J. CAO[1], G. AHMADI[1] AND M. MASSOUDI[2]

[1] Department of Mechanical and Aeronautical Engineering, Clarkson University, Potsdam, NY 13699-5725, USA

[2] US Department of Energy, Pittsburgh Energy Technology Center, PO Box 10940, Pittsburgh, PA 15236-0940, USA

(Received 21 October 1993 and in revised form 24 January 1996)

Gravity-driven granular flow of slightly frictional particles down an inclined, bumpy chute is studied. A modified kinetic model which includes the frictional energy loss effects is used, and the boundary conditions for a bumpy wall with small friction are derived by ensuring the balance of momentum and energy. At the free surface, the condition of vanishing of the solid volume fraction is used. The mean velocity, the fluctuation kinetic energy and the solid volume fraction profiles are evaluated. It is shown that steady granular gravity flow down a bumpy frictional chute could be achieved at arbitrary inclination angles. The computational results also show that the slip velocity may vary considerably depending on the granular layer height, the surface boundary roughness, the friction coefficient and the inclination angles. The model predictions are compared with the existing experimental and simulation data, and good agreement is observed. In particular, the model can well predicate the features of the variation of solid volume fraction and fluctuation energy profiles for different particle–wall friction coefficients and wall roughnesses.

1. Introduction

The inclined chute serves as an important component of many industrial solids transport processes in addition to providing a bench mark for comparison of theoretical predictions with experimental data. Because of its significance, granular gravity flows have been the subject of a number of investigations. Over the past two decades, theoretical analysis of gravity-driven rapid particulate flows have been performed by Savage (1979), Ma & Ahmadi (1985), Richman & Marciniec (1990), Johnson, Nott & Jackson (1990), Anderson & Jackson (1992), Gudhe, Rajagopal & Massoudi (1994), Abu-Zaid & Ahmadi (1993) and Oyediran *et al.* (1994). Using the molecular dynamics procedure, Campbell & Brennen (1985), Walton *et al.* (1988) and Walton (1992) presented digital simulation results for granular flow properties such as solid volume fraction, velocity and fluctuation kinetic energy (granular temperature) for chute flows. These computer simulations also provided insights into the mechanisms that govern the rapid flow of granular materials. Experimental studies of granular gravity flows were reported by Augenstein & Hogg (1978), Savage (1978, 1979), Campbell, Brennen & Sabersky (1985), Drake & Shreve (1986), Patton, Brennen & Sabersky (1987), Johnson *et al.* (1990) and Drake (1990, 1990) among others. The experimental data for solid volume fraction and velocity profiles provided by these studies play a vital role in verifying the existing models.

While considerable progress toward understanding the behaviour of granular gravity flows has been made, most earlier models were limited to frictionless, slightly inelastic particles and a specific flow regime. However, many flows of practical interest fall into the intermediate flow regime where both frictional contacts and particle-particle collisions are significant. Johnson *et al.* (1990) did account for the effects of enduring frictional contact in their works by adding the Coulomb friction law to the granular kinetic and collisional stresses in their study of gravity flows. This model essentially combines the available constitutive theories for rapid and slow granular flows through a linear superposition. Abu-Zaid & Ahmadi (1990) developed a kinetic model which incorporated the effect of frictional energy losses during collisions. Cao & Ahmadi (1995) used this model to analyse granular Couette flows and the results showed that the effect of frictional energy losses is significant.

Solid wall boundary conditions for rapid granular flows were studied by Hui *et al.* (1984) using heuristic momentum and energy balance equations. Similar boundary conditions for disk flows were described by Pasquarell *et al.* (1988). Ma & Ahmadi (1985) and Abu-Zaid & Ahmadi (1993) also analysed shear flows of granular materials using semi-empirical boundary conditions. These studies showed that the no-slip boundary condition is reasonable only when the boundary surface is sufficiently rough. Jenkins & Richman (1985) developed a set of kinetic-based boundary conditions for two-dimensional smooth circular disk flows in the neighbourhood of a bumpy wall. Later this work was extended to flows of spherical particles by Richman (1988) and Hanes, Jenkins & Richman (1988). More recently, Jenkins (1992) proposed a set of boundary conditions for rapid granular flows over a flat, frictional wall.

For the free surface boundary condition, most earlier works assumed that the stress and the energy flux vanish at a finite height (for which the solid volume fraction need not be zero). Such a free surface boundary condition, while avoiding the stiffness problem in the numerical solution, is obviously not exact. In reality, granular layer height continues until the condition of zero solid volume fraction is reached. Recently, using the momentum and energy balance at the interface between colliding and freely flying grains, Jenkins & Hanes (1993) developed a boundary condition for granular temperature (fluctuation kinetic energy).

In this paper, a kinetic model that incorporates frictional energy losses is used to analyse the steady, fully developed gravity-driven rapid granular flows down a bumpy, frictional inclined surface. The modified kinetic-based boundary condition of Richman (1988) that accounts for the frictional energy losses due to interactions between the grains and the boundaries is derived and used in the analysis. On the free surface, the boundary condition that allows for the height to continue to the point of zero solid volume fraction is applied. The particles are treated as identical, nearly elastic and slightly frictional spheres. Variation between particle–particle and particle–wall collisional properties is also allowed in the model. An iterative computational procedure is developed and is used to solve the equations of motion. The predicted velocity, solid volume fraction and fluctuation kinetic energy profiles for different inclination angles, flow heights, friction coefficients and surface boundary geometry (roughness) are presented in graphical forms. It is shown that, with the new wall and free surface boundary conditions, the model predictions are in good agreement with the available experimental data and molecular dynamics simulations results. The effects of frictional energy losses on the shape of solid volume fraction and fluctuation kinetic energy profiles are also discussed.

2. Governing equations

The equations governing the motion of granular materials during rapid flows are: conservation of mass

$$\frac{\partial \rho}{\partial t} + \frac{\partial(\rho u_i)}{\partial x_i} = 0; \tag{1}$$

balance of momentum

$$\rho \frac{\mathrm{d}u_i}{\mathrm{d}t} = \rho b_i + \frac{\partial \tau_{ij}}{\partial x_j}; \tag{2}$$

conservation of energy

$$\rho \frac{\mathrm{d}k}{\mathrm{d}t} = -\frac{\partial K_j}{\partial x_j} + \tau_{ji}\frac{\partial u_i}{\partial x_j} - \rho\epsilon. \tag{3}$$

Here u_j is the mean velocity vector, ρ is the mass density, τ_{ij} is the stress tensor, K_j is the fluctuation energy flux vector, k is the fluctuation energy per unit mass, and ϵ is the collisional dissipation rate per unit mass. For rough spherical particles with small friction coefficient, the disspation rate is given by Abu-Zaid & Ahmadi (1990):

$$\epsilon = a_0 \chi k^{3/2}, \tag{4}$$

$$a_0 = \alpha_0 \nu(1+r)(1-r+2\mu)/d, \tag{5}$$

where r is the coefficient of restitution, μ is the coefficient of friction, d is the particle diameter, ν is the solid volume fraction, $\alpha_0 = 3.908$ is a constant, and χ is the radial distribution function given by Ahmadi & Ma (1986):

$$\chi = \frac{1 + 2.5\nu + 4.59\nu^2 + 4.52\nu^3}{[1-(\nu/\nu_m)^3]^{0.678}} \tag{6}$$

in which $\nu_m = 0.644$ is the limiting maximum solid volume fraction.

The constitutive equations as given by Abu-Zaid & Ahmadi (1990) are used in this study. Accordingly, the stress tensor is given as

$$\tau_{ij} = -\left(P + \frac{2}{3}\rho k^{1/2}\frac{\partial u_k}{\partial x_k}\right)\delta_{ij} + \beta k^{1/2}\left(\frac{\partial u_i}{\partial x_j} + \frac{\partial u_j}{\partial x_i}\right) \tag{7}$$

where

$$P = \tfrac{1}{3}\rho k[2(1+4\nu\chi) + (1+r)(1-r+2\mu)], \tag{8}$$

$$\beta = \beta_0 f_1(\nu), \qquad \beta_0 = 0.0853\rho_0 d, \tag{9}$$

$$f_1(\nu) = \chi^{-1} + 3.2\nu + 12.18\nu^2\chi, \tag{10}$$

in which ρ_0 is the density of grains and $\rho = \rho_0\nu$.

The energy-flux vector K_i given by Abu-Zaid & Ahmadi (1990) is

$$K_i = -\kappa k^{1/2}\left[\frac{\partial k}{\partial x_i} - \frac{(1+r)(1-r+2\mu)}{1+r^2}\frac{k}{\nu}\frac{\partial \nu}{\partial x_i}\right] \tag{11}$$

where

$$\kappa = \tfrac{5}{6}\beta_0(1+r^2)(\chi^{-1} + 4.8\nu + 12.12\nu^2\chi). \tag{12}$$

This completes the summary of the governing equations.

The kinetic formulation outlined is applicable to cases where the friction coefficient is small so that slip during collision occurs and the rotational effects of particles

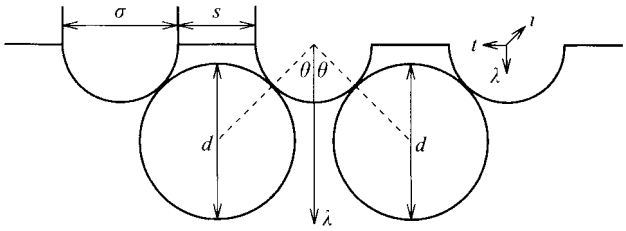

FIGURE 1. Geometry of the bumpy boundary.

are insignificant. The theory is not intended for analysing flows of highly frictional granules, for which the effects of particle rotation and contact forces due to the enduring friction become important. In Appendix A, it is shown that the ratio of rotational fluctuation kinetic energy to the translational fluctuation kinetic energy is of the order of μ^2. Furthermore, according to Lun & Savage (1987), for an infinitely large frictional coefficient (when the slip velocity is zero), the rotational energy is less than 25% of the translational energy. Therefore, neglecting the rotational effects of particles for small frictional coefficient does not lead to a significant error.

3. Boundary conditions at wall the and free surfaces

In order to solve equations (1)–(3) for realistic flows, proper boundary conditions must be prescribed. For granular flows, the experimental and digital simulation results indicate that occurrence of slip at the wall is a common feature. It is now well understood that the flow behaviour at surface boundaries is an integral part of the solution for the entire flow field. Because of the slip velocity, a solid boundary performs shear work and generates granular fluctuation kinetic energy at a rate equal to the product of the wall shear stress and the slip velocity. At the same time, particulate collisions with the wall lead to energy dissipation D. In addition, the collisions of the flow particles with the solid boundary generate a flow momentum deficiency $\boldsymbol{M}$. For a unit area of a boundary that interacts with the flow and has a unit inward normal $\boldsymbol{\lambda}$, the balance of momentum at the boundary requires that

$$\boldsymbol{M} = \boldsymbol{\lambda} \cdot \boldsymbol{\tau} \tag{13}$$

and the statement of conservation of energy becomes

$$\boldsymbol{M} \cdot \boldsymbol{v} - D = \boldsymbol{K} \cdot \boldsymbol{\lambda} \tag{14}$$

where $\boldsymbol{v} = \boldsymbol{V}_b - \boldsymbol{u}_w$ is the slip velocity with $\boldsymbol{V}_b$ being the boundary velocity and $\boldsymbol{u}_w$ the flow velocity at the wall.

Expressions for $\boldsymbol{M}$ and D depend on the details of the geometry of the boundary surface. For the bumpy boundary shown in figure 1, the expressions are evaluated in Appendix B, and are

$$D = \frac{8}{3(3\pi)^{1/2}}(1 - r_w + 2\mu_w)\omega\rho k^{3/2}(1 - \cos\theta)\operatorname{cosec}^2\theta, \tag{15}$$

$$M_i = \tfrac{2}{3}\omega\rho k \left\{ \lambda_i + (2v_i/(3\pi k)^{1/2})[2\operatorname{cosec}^2\theta(1 - \cos\theta) - \cos\theta], \right.$$
$$\left. + \left(\frac{3}{\pi k}\right)^{1/2} \sigma_0 \frac{\partial u_k}{\partial x_j}\left[\left(1 + B\frac{\sigma}{\sigma_0}\right) I_{ijk} + \lambda_j I_{ik}\right]\right\} \tag{16}$$

where

$$B = \pi(1 + 5/8\nu\chi)/12\sqrt{2}, \quad \sigma_0 = (\sigma + d)/2, \quad \theta = \arcsin\left(\frac{1+\hat{d}}{1+\hat{s}}\right) \tag{17}$$

with

$$\hat{d} = d/\sigma, \quad \hat{s} = s/\sigma \tag{18}$$

and

$$I_{ij} = \tfrac{2}{3}\{2[\mathrm{cosec}^2\theta(1-\cos\theta)+\cos\theta]\lambda_i\lambda_k+[2\,\mathrm{cosec}^2\theta(1-\cos\theta)-\cos\theta](\iota_i\iota_k+t_it_k)\}, \tag{19}$$

$$I_{ijk} = (\sin^2\theta - 2)\lambda_i\lambda_j\lambda_k - \tfrac{1}{2}\sin^2\theta[\lambda_i(\iota_j\iota_k + t_jt_k) + \lambda_j(\iota_k\iota_i + t_kt_i) + \lambda_k(\iota_i\iota_j + t_it_j)]. \tag{20}$$

Here, $t = (t_i,\ t_j,\ t_k)$, $\iota = (\iota_i,\ \iota_j,\ \iota_k)$, and $\lambda = (\lambda_i,\ \lambda_j,\ \lambda_k)$ form an orthonormal triad as shown in figure 1, r_w is the coefficient of restitution between particles and the wall, μ_w is the friction coefficient of the wall, v_i is the slip velocity component, and ω is a factor that accounts for the effects of excluded area (collisional shielding) on the frequency of collisions and the average solid volume fraction. Note that equation (15) is a modified version of the one given by Richman (1988) as suggested by Cao & Ahmadi (1995) to account for the wall frictional energy losses. This equation was obtained by assuming that there is frictional slip during the particle collision with the wall. Clearly, when $r_w = 1$, equation (15) shows that there is a dissipation of energy due to frictional slip. This boundary condition is applicable to particles with small friction coefficient for which slip during collision occurs, and the particle rotational effect is negligible.

In Appendix B, a detailed derivation of boundary conditions for a slightly frictional bumpy wall is presented. For small friction coefficients, the results are identical to equations (15) and (16) with a factor of $\pi/4$ being taken as unity.

To ensure that no particle ever collides with the flat part of the wall, $\hat{d}$ must be less than $-1 + (1 + 2\hat{s})^{1/2}$. The angle θ in the above equations is a natural measure of the wall roughness. By increasing $\hat{d}$ or decreasing $\hat{s}$, additional surface area of the wall becomes available for collisions, and consequently the boundary becomes effectively more rough.

For the flat frictional boundary, at the free surface the energy flux must vanish. That implies

$$\boldsymbol{\lambda} \cdot \boldsymbol{K} = 0. \tag{21}$$

Furthermore, the stress-free surface conditions require that the total normal and tangential stresses acting at the free surface vanish:

$$\boldsymbol{\lambda} \cdot \boldsymbol{t} \cdot \boldsymbol{\tau} = 0, \tag{22}$$

$$\boldsymbol{\lambda} \cdot \boldsymbol{\lambda} \cdot \boldsymbol{\tau} = 0. \tag{23}$$

The elevation of the free surface is obtained from the condition that the solid volume fraction becomes zero.

The experimental results of Drake & Shreve (1986) and others show that there is a saltation zone near the free surface. In this region, the solid volume fraction is quite low and decreases toward the diffuse free surface. The numerical calculation in this region often indicates that the stress retains quite large values to within a fraction of a particle diameter of the nominal free surface, after which it drops rapidly to zero. This introduces a stiffness problem into the numerical solution. In order to avoid this difficulty, some authors abandoned satisfying the stress-free condition and used some approximating assumptions at the free surface. However, these often led

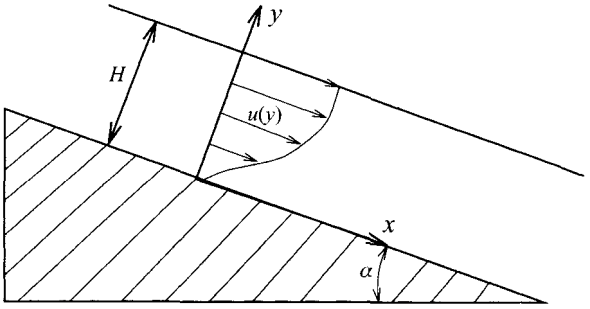

FIGURE 2. Gravity flow down an inclined chute.

to inaccuracy in the solutions (Johnson *et al.* 1990). The present paper shows that as long as a proper grid and numerical algorithm are adopted, the numerical difficulty caused by using the stress-free conditions may be avoided.

4. Steady gravity granular flow

In this section, the special case of gravity granular flows down an inclined bumpy chute with an inclination angle α as shown in figure 2 is analysed. It is assumed that the distance from the incline to the free surface is H (which itself is generally an unknown). A Cartesian coordinate system with y being the distance from the lower wall is used. For a steady, fully developed flow, it may be assumed that

$$\left.\begin{aligned} \boldsymbol{u} = [u(y),\ 0,\ 0],\quad k = k(y),\quad v = v(y),\quad \boldsymbol{K} = [0,\ K_2(y),\ 0], \\ \boldsymbol{\tau} = \begin{pmatrix} \tau_{xx}(y) & \tau_{xy}(y) & 0 \\ \tau_{yx}(y) & \tau_{yy}(y) & 0 \\ 0 & 0 & \tau_{zz}(y) \end{pmatrix}, \end{aligned}\right\} \tag{24}$$

where $u(y)$ is the mean velocity along the incline, and $\tau_{xy} = \tau_{yx}$.

For simplicity, let

$$N = \tau_{yy},\quad S = -\tau_{xy} \tag{25}$$

and introduce the following non-dimensional variables:

$$\left.\begin{aligned} \eta = \frac{y}{d},\ \hat{u} = \frac{u}{(dg)^{1/2}},\ \hat{\epsilon} = \frac{\rho\epsilon}{\rho_0(dg)^{3/2}/d},\ \hat{k} = \frac{k}{dg},\ w = \hat{k}^{1/2},\ \hat{v}_x = \frac{v_x}{(dg)^{1/2}}, \\ \hat{K} = \frac{K_2}{\rho_0(dg)^{3/2}},\ \hat{N} = \frac{N}{\rho_0 dg},\ \hat{S} = \frac{S}{\rho_0 dg}. \end{aligned}\right\} \tag{26}$$

Here g is the vertical acceleration due to gravity.

Substituting equations (4)–(12), and (24)–(26) into (1)–(3), the balance of mass (1) and the z-component of the balance of momentum (2) are satisfied identically. The x- and y-components of the momentum equation and statement of balance of fluctuation energy, respectively, become

$$\mathrm{d}\hat{N}/\mathrm{d}\eta = -\nu\cos\alpha, \tag{27}$$

$$\mathrm{d}\hat{S}/\mathrm{d}\eta = -\nu\sin\alpha, \tag{28}$$

$$\mathrm{d}\hat{K}/\mathrm{d}\eta - \hat{S}\,\mathrm{d}\hat{u}/\mathrm{d}\eta + \hat{\epsilon} = 0, \tag{29}$$

where

$$\hat{N} = \nu w^2 F_0(\nu), \tag{30}$$

$$\hat{S} = F_1(\nu) w \mathrm{d}\hat{u}/\mathrm{d}\eta, \tag{31}$$

$$\hat{\epsilon} = \hat{N} w F_2(\nu), \tag{32}$$

$$\hat{K} = -F_3(\nu)\hat{N}\mathrm{d}w/\mathrm{d}\eta, \tag{33}$$

in which functions F_i are defined as

$$F_0(\nu) = \tfrac{1}{3}[2(1+4\mu\chi) + (1+r)(1-r+2\mu)], \tag{34}$$

$$F_1(\nu) = 0.0853 f_1(\nu), \tag{35}$$

$$F_2(\nu) = \alpha_0 \nu\chi[1 - r^2 + 2\mu(1+r)]/F_0(\nu), \tag{36}$$

$$F_3(\nu) = \frac{0.1422(1+r^2)(\chi^{-1} + 4.8\nu + 12.12\nu\chi)}{\nu F_0(\nu)}. \tag{37}$$

Note that in equation (2), the diffusion of energy due to the concentration gradient is neglected.

From (30), (31), one finds

$$\frac{\mathrm{d}\hat{u}}{\mathrm{d}\eta} = \frac{\nu w F_0}{F_1}\frac{\hat{S}}{\hat{N}}. \tag{38}$$

Using the expressions for $\hat{N}$, $\hat{S}$, $\hat{\epsilon}$ $\hat{K}$, and $\mathrm{d}\hat{u}/\mathrm{d}\eta$, as given by (30)–(33) and (38) in equation (29), the final form of the energy equation follows:

$$\frac{\mathrm{d}}{\mathrm{d}\eta}\left(\hat{N}F_3\frac{\mathrm{d}w}{\mathrm{d}\eta}\right) - w\hat{N}\left[F_2 - \frac{\nu F_0}{F_1}\left(\frac{\hat{S}}{\hat{N}}\right)^2\right] = 0. \tag{39}$$

4.1. *Boundary conditions*

At the free surface ($\eta = \hat{H}$), the following boundary conditions must be satisfied:

$$\nu = 0, \tag{40}$$

$$\hat{S} = 0, \quad \hat{K} = 0, \tag{41}$$

where $\hat{H} = H/d$ is the non-dimensional flow height. Equations (40) and (41) imply that the normal stress $\hat{N}$ and gradient of fluctuation energy ($\mathrm{d}w/\mathrm{d}\eta$) are zero at the free surface.

At the base ($\eta = 0$), the velocity boundary condition is

$$\hat{u} = \hat{v}_x. \tag{42}$$

Using the non-dimensional variables, the momentum boundary condition (13) at the wall may be restated as

$$\hat{N} = \tfrac{2}{3}\omega\nu_w w_w^2, \tag{43}$$

$$\hat{S} = \omega\nu_w w_w\left(\hat{v}_x G_1 + \frac{\mathrm{d}\hat{u}_w}{\mathrm{d}\eta}G_2\right), \tag{44}$$

where

$$G_1 = \frac{4}{3(3\pi)^{1/2}}[2\mathrm{cosec}^2\theta(1-\cos\theta) - \cos\theta], \tag{45}$$

$$G_2 = \frac{2}{(3\pi)^{1/2}}\frac{\sigma_0}{\sigma}\left\{\tfrac{1}{2}\left(1 + \frac{\sigma}{\sigma_0}B\right)\sin^2\theta - \tfrac{2}{3}[2\mathrm{cosec}^2\theta(1-\cos\theta) - \cos\theta]\right\}. \tag{46}$$

The energy boundary condition (14) now becomes

$$\hat{S}\hat{v}_x - \omega C_w \nu_w w_w^3 = 2F_3(\nu_w) w_w^2 (\mathrm{d}w/\mathrm{d}\eta)_w \tag{47}$$

where

$$C_w = \frac{8}{3(3\pi)^{1/2}}(1 - r_w + 2\mu_w)(1 - \cos\theta)\mathrm{cosec}^2\theta. \tag{48}$$

In these equations, the subscript w denotes the value of a variable at the wall.

Eliminating ω from the boundary conditions (43), (44) and (47) and using the equation (30) for the normal stress, the momentum and energy boundary conditions, respectively, become

$$\hat{v}_x = \frac{2w_w}{3G_1}\left[1 - \frac{3\nu_w F_0(\nu_w)}{2F_1(\nu_w)}G_2\right]\frac{\hat{S}}{\hat{N}} \tag{49}$$

and

$$\left(\frac{\mathrm{d}w}{\mathrm{d}\eta}\right)_w = \frac{1}{F_3(\nu_w)}\left[\left(\frac{\hat{S}}{\hat{N}}\right)\hat{v}_x - \tfrac{3}{2}C_w w_w\right] \tag{50}$$

Note that Jenkins (1992) proposed an interesting boundary condition for a frictional flat surface. For the limit of small frictional coefficients (sliding case), Jenkins' boundary condition reduces to $\hat{S}/\hat{N} = \mu_w$. The equations of balance of momentum as given by (27) and (28) then imply that steady-state gravity flow is possible only for the inclination angle of $\alpha = \tan^{-1}\mu_w$ (this is an obvious result for a rigid block sliding down an incline). Therefore, to achieve steady flows at inclination angles other than $\tan^{-1}\mu_w$, a small amount of surface roughness (bumps) is required. The other option is to include the effect of sustained multiple contacts among particles in the model (e.g. as suggested by Johnson *et al.* 1990). In this paper, only the consequence of the first alternative is explored.

5. Computational model

For convenience in the numerical solutions, equation (27) is integrated from η to $\hat{H}$ and gives

$$\nu F_0(\nu) w^2 = -\int_\eta^{\hat{H}} \nu \cos\alpha \mathrm{d}\eta. \tag{51}$$

It should also be pointed out that regardless of the distribution of $\nu(\eta)$, from equations (27), (28) and boundary condition (40) and (41), it follows that

$$\frac{\hat{S}}{\hat{N}} = \tan\alpha = \text{const.} \tag{52}$$

It is also recognized that there are rather large velocity and solid volume fraction gradients near the solid wall and the free surface. To avoid the stiffness problem in the numerical computation and obtain accurate solutions in these critical regions, the grid coordinates are selected by using

$$\eta_j = \tfrac{1}{2}\hat{H}\left[1 - \cos\frac{(j-1)\pi}{n-1}\right] \quad j = 1,\ 2,\ 3,\ \cdots,\ n. \tag{53}$$

This allows for a dense distribution of grid point near the boundaries. Here a total of 150 grid points are used.

Using the standard, second-order-accurate, central finite difference for the second derivative at every grid point, equations (38) and (39) lead to

$$\left(\frac{\mathrm{d}\hat{u}}{\mathrm{d}\eta}\right)^{(k+1)} = \left(\frac{v}{F_1}\frac{\hat{S}}{\hat{N}}\right)^{(k+1)} w^{(k+1)}, \tag{54}$$

$$a w_{j-1}^{(k+1)} - b w_j^{(k+1)} + c w_{j+1}^{(k+1)} = 0 \quad j = 2,\ 3,\ \cdots,\ n-1, \tag{55}$$

where a, b and c have the following expressions:

$$a = \frac{1}{h_{j-1}(h_{j-1}+h_j)}(F_{3j-1}\hat{N}_{j-1} + F_{3j}\hat{N}_j)^{(k)}, \tag{56}$$

$$b = \frac{1}{h_{j-1}(h_{j-1}+h_j)}(F_{3j-1}\hat{N}_{j-1} + F_{3j}\hat{N}_j)^{(k)} + \frac{1}{h_j(h_j+h_{j-1})}(F_{3j}\hat{N}_j + F_{3j+1}\hat{N}_{j+1})^{(k)} + \left[\hat{N}_j\left(F_{2j} - \frac{v_j F_{0j}}{F_{1j}}\left(\frac{\hat{S}}{\hat{N}}\right)^2\right)\right]^{(k)}, \tag{57}$$

$$c = \frac{1}{h_j(h_j+h_{j-1})}(F_{3j}\hat{N}_j + F_{3j+1}\hat{N}_{j+1})^{(k)}. \tag{58}$$

In equations (53)–(58), the subscript j identifies the grid point in the finite difference mesh, the superscript k denotes the order of iteration and $h_j = \eta_{j+1} - \eta_j$ is the spatial increment.

Boundary conditions (41), (49) and (50) lead to

$$\left[\frac{3C_w}{2F_5(v_1)} + \frac{1}{h_1}\right]^{(k)} w_1^{(k+1)} + \frac{1}{h_1} w_2^{(k+1)} = \left(\frac{\hat{v}_x}{F_5(v_1)}\right)^{(k)} \frac{\hat{S}}{\hat{N}}, \tag{59}$$

$$w_n^{(k+1)} - w_{n-1}^{(k+1)} = 0, \tag{60}$$

$$(\hat{v}_x)^{(k+1)} = \left\{\frac{2w_1}{3G_1}\left[1 - \frac{3v_n F_0(v_n)}{2F_1(v_n)} G_2\right]\right\}^{(k+1)} \frac{\hat{S}}{\hat{N}}, \tag{61}$$

where subscript 1 stands for the first (wall) grid point, and n stands for the last (free surface) grid point.

Using the trapezoidal rule, equation (51) may be restated as

$$[v_j F(v_j) w_j^2]^{(k+1)} = -\tfrac{1}{2}\cos\alpha \sum_{i=j}^{n-1} [h_i(v_i + v_{i+1})]^{(k+1)} \quad j = 1,\ 2,\ 3,\ \cdots,\ n-1 \tag{62}$$

in which $v_n = 0$.

The iterative scheme of solution uses the following steps:

(i) At the initial step $k = 0$, the initial approximate values of $\hat{v}_x^{(0)}$, $v_j^{(0)}$, $u_j^{(0)}$ and $w_j^{(0)}$ ($j = 1,\ 2,\ \cdots,\ n$) are specified.

(ii) Equations (55), (59) and (60) are used to find $w_j^{(k+1)}$ ($j = 1,\ 2,\ 3,\ \cdots,\ n$).

(iii) Using the Newton–Raphson iterative method, equation (62) is solved for $v_j^{(k+1)}$ ($j = 1,\ 2,\ 3,\ \cdots,\ n-1$).

(iv) Equation (61) is then used to evaluate $v_x^{(k+1)}$.

(v) A fourth-order Runge–Kutta scheme is used for evaluating $u_j^{(k+1)}$ ($j = 1,\ 2,\ 3, \cdots,\ n$) from equation (54).

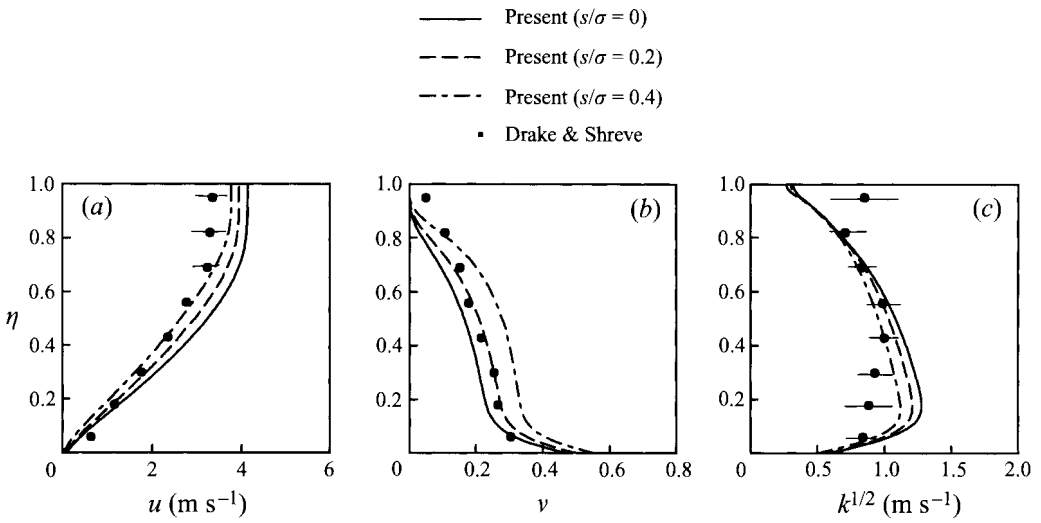

FIGURE 3. Variations of (*a*) mean velocity, (*b*) solid volume fraction and (*c*) SR-fluctuation kinetic energy profiles for a gravity flow with $\alpha = 42.75°$, $r_w = r = 0.84$, $\mu_w = \mu = 0.41$, $\hat{s} = 0.4$, $\hat{d} = 1$, $H/d = 16$. Comparison with the results of Drake & Shreve.

(vi) Steps (ii) to (v) are repeated until values of $\hat{v}_x$, v_j, u_j, w_j ($j = 1, 2, \cdots, n$) converge.

If the changes in the variables are everywhere less than 10^{-4} of their absolute values between two consecutive iterations, the solutions are considered to be converged.

It is found that convergence can be rapidly reached by the use of an over-relaxation method. That is, the new values of $w_j^{(k+1)}$, $v_j^{(k+1)}$ and $\hat{v}^{(k+1)}$ are obtained by the following linear combinations:

$$\left.\begin{aligned} w_j^{(k+1)} &= (1 - \Theta_w) w_j^{(k)} + \Theta_w (w_j^{(k+1)})_c, \quad (63)\\ v_j^{(k+1)} &= (1 - \Theta_v) v_j^{(k)} + \Theta_v (v_j^{(k+1)})_c, \quad (64)\end{aligned}\right\} j = 1, 2, 3, \cdots, n,$$

$$\hat{v}_x^{(k+1)} = (1 - \Theta_v) \hat{v}_x^{(k)} + \Theta_v (\hat{v}_x^{(k+1)})_c, \quad (65)$$

where Θ_w, Θ_v, Θ_v are relaxation coefficients, and the subscript c denotes the calculated values of variables after $k + 1$ iterations.

6. Results and discussion

For several inclination angles, granular layer heights and material properties, granular flows down a bumpy inclined chute are studied, and the mean velocity, solid volume fraction and square-root (SR) fluctuation kinetic energy profiles are evaluated. The results are presented in graphical form and discussed.

In order to test the present model, we first compare the predicted mean velocity, solid volume fraction and SR-fluctuation kinetic energy profiles with the experimental data of Drake & Shreve (1986) for an inclination angle of $\alpha = 42.75°$ in figure 3. Drake & Shreve's experiment was carried out in an inclined glass-walled channel 3.7 m long and 6.5 mm wide using 6 mm diameter cellulose-acetate spherical particles. The bed consisted of spheres like those in the flows, which were glued with random spacing of 0 to 5 mm to an aluminium bar. A granular layer height of H/d=16, $\hat{d} = 1$, $r = r_w = 0.84$ and $\mu = \mu_w = 0.4$ as were given in the experiment are assumed in the present analysis.

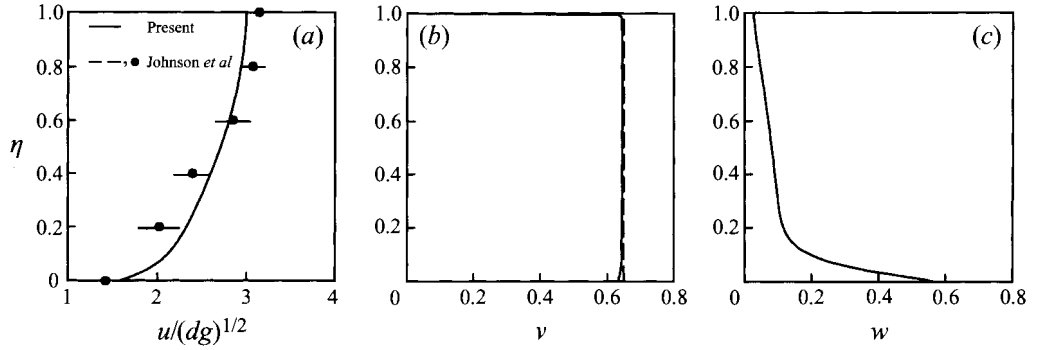

FIGURE 4. Variations of (*a*) mean velocity, (*b*) solid volume fraction and (*c*) SR-fluctuation kinetic energy profiles for a gravity flow with $\alpha = 17°$, $r = r_w = 0.9$, $\mu = \mu_w = 0.45$, $H/d = 20$. Comparison with the results of Johnson *et al.*

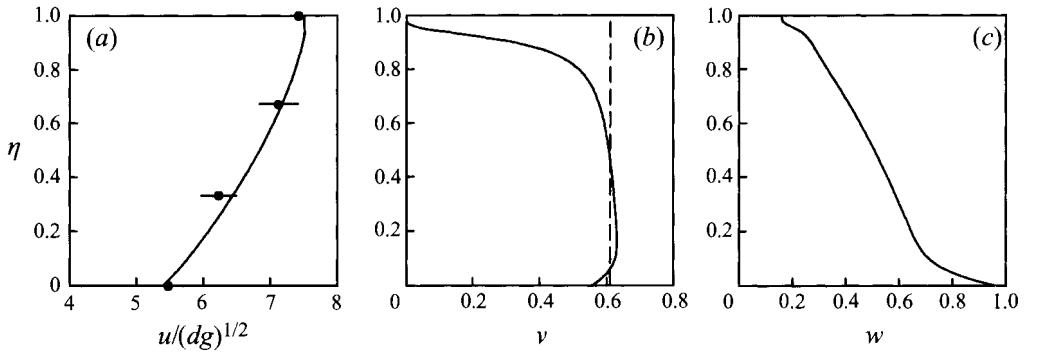

FIGURE 5. As figure 4 but for $H/d = 6$.

To simulate the randomly spaced gaps between the wall particles, three different values of $\hat{s} = 0$, 0.2 and 0.4 are used and the corresponding computed mean velocity, solid volume fraction and SR-fluctuation kinetic energy profiles are presented in figure 3. For comparison, the two-dimensional solid volume fraction ν_{2D} of Drake & Shreve is converted into the equivalent three-dimensional data using $\nu_{3D}=4\nu_{2D}^{3/2}/3\pi^{1/2}$, as was suggested by Campbell & Gong (1986), and the results are shown in figure 3(*b*). In figure 3(*c*), the granular temperature, T, of Drake & Shreve is converted into fluctuation kinetic energy using $k = 3T/2$. Figure 3 shows that the predicted velocity and solid volume fraction profiles are in reasonable agreement with the experimental data. In particular, the monotonic increasing trend of ν toward the wall and the small amount of slip velocity are well predicted by the model. The model, however, overestimates the experimental data for the SR-fluctuation kinetic energy near the wall. As noted before, the experiment was performed for a monolayer of granular particles in a two-dimensional channel, while the present model predictions are for a fully three-dimensional particulate flow. Therefore, certain deviations should be expected.

Johnson *et al.* (1990) also performed a series of experiments for gravity flow of 1 mm diameter glass beads down an inclined chute with a smooth aluminium plate. The chute was 1.4 m long and 6.35 cm wide, and was bounded by vertical glass walls 12.7 cm high. Their mean velocity data for an inclination angle of $\alpha = 17°$ and $H/d = 20$ are reproduced in figure 4. The present model predictions for the same

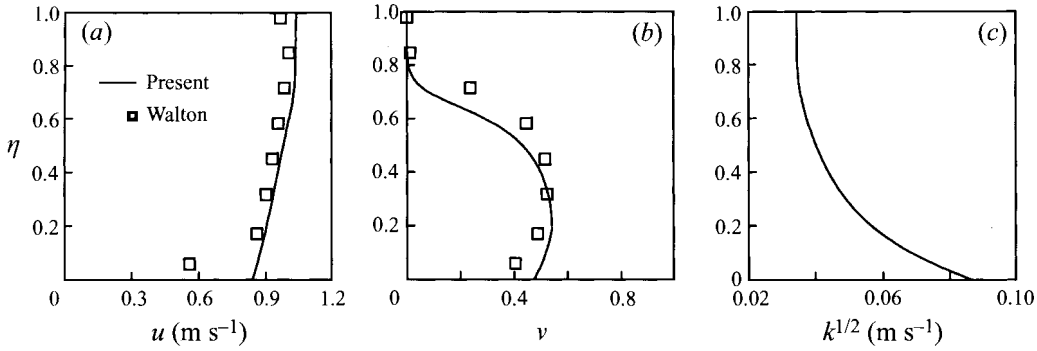

FIGURE 6. Non-dimensional (*a*) mean velocity, (*b*) solid volume fraction and (*c*) SR-fluctuation kinetic energy profiles for a gravity chute flow with $\alpha = 17°$, $\hat{s} = 0$, $\hat{d} = 10$, $r = r_w = 0.85$, $\mu = \mu_w = 0.4$, $H/d = 9$. Comparison with the simulation results of Walton (1992).

conditions are also plotted in this figure for comparison. Here $r = 0.91$ and $\mu = 0.45$ for glass beads as suggested by Johnson *et al.* (1990) are used in the numerical simulation. The smooth wall surface is simulated by taking the wall parameters as $\hat{s} = 0$ and $\hat{d} = 10$. Thus, the bumps on the wall are one tenth the size of the grains in the flow and are tightly packed. Figure 4(*a*) shows that the calculated velocity profile is in good agreement with the experimental data. The predicted slip at the wall, however, is slightly higher than that observed in the experiment.

From figure 4(*b*), it is observed that the solid volume fraction remains almost a constant across the chute with a sharp gradient near the free surface. The dashed line in this figure corresponds to the mean solid volume fraction of 0.65 reported in the experiment of Johnson *et al.* (solid volume fraction and fluctuation kinetic energy profiles were not measured). The predicted mean solid volume fraction here is $\bar{\nu} = 0.641$ which is quite close to the experimental value.

The variation of SR-fluctuation kinetic energy over the incline is shown in figure 4(*c*). It is observed that the SR-fluctuation energy has a large value near the wall and decreases rapidly to about 20% of its wall value at a distance of $0.2\hat{H}$. It then decreases gradually toward the free surface. Unfortunately, there are no experimental data for the fluctuation kinetic energy for comparison in this case.

Figure 5 presents the model predictions for $H/d = 6$ and a comparison with the corresponding experimental data of Johnson *et al.* (1990). The rest of parameters used in this simulation are the same as those of figure 4. Figure 5(*a*) shows that the calculated velocity profile is in reasonable agreement with the experimental data. A significant amount of slip at the wall is also noticed in the experiment which is well predicted by the model. The calculated solid volume fraction profile in figure 5(*b*) remains roughly a constant, except for its rapid decrease in the saltation region and a decreasing trend in the shearing zone near the wall. The calculated mean solid volume fraction is $\bar{\nu} = 0.547$, while the experimentally reported value was about 0.61. Figure 5(*c*) shows the SR-fluctuation kinetic energy profile has a large value near the wall and decreases with distance from the chute surface. Based on the general agreement of the model predictions with the experimental data in figure 5 one can conclude that the (continuum) model equations are applicable to cases with surprisingly low H/d ratios.

Using a molecular dynamic method (MD), Walton (1992) studied gravity flows of 1 mm diameter frictional spheres on a frictional 17° incline. His simulation results

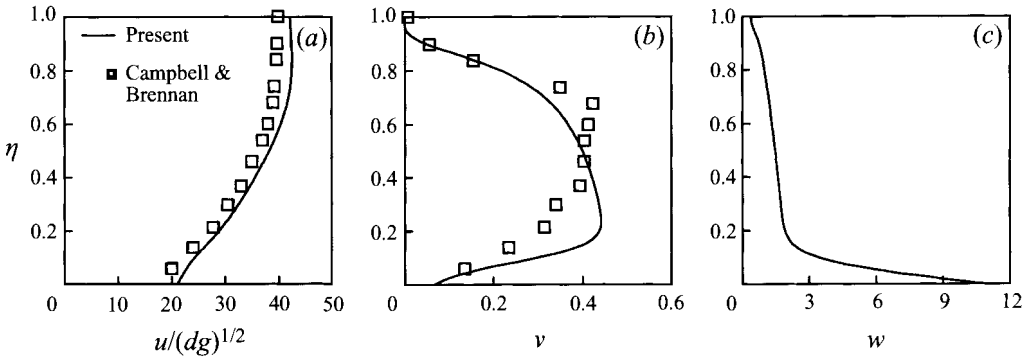

FIGURE 7. Non-dimensional (*a*) mean velocity, (*b*) solid volume fraction and (*c*) SR-fluctuation kinetic energy profiles for a gravity chute flow with $\alpha = 30°$, $\hat{s} = 0$, $\hat{d} = 2$, $r_w = 0.8$, $r = 0.6$, $\mu = \mu_w = 0$, $H/d = 25$. Comparison with the simulation results of Campbell & Brennen (1985).

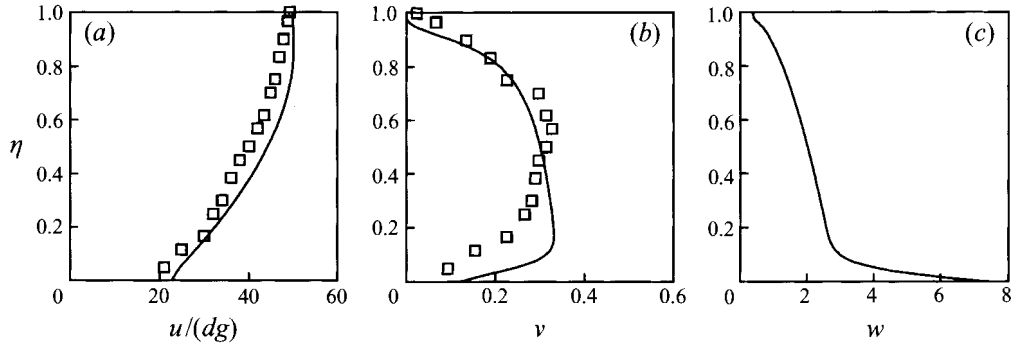

FIGURE 8. As figure 7 but for $r = 0.8$, $H/d = 30$.

for the mean velocity and solid volume fraction profiles are reproduced in figure 6. The corresponding fluctuation kinetic energy profile was not reported by Walton. The present model predictions for $H/d = 9$, $r = r_w = 0.85$ and $\mu = \mu_w = 0.4$ which are identical to those used by Walton are also plotted in this figure for comparison. The flat frictional wall considered in Walton's simulation is modelled as bumpy boundary conditions with $\hat{s} = 0$ and $\hat{d} = 10$. That is, the wall particles are ten times smaller than the flow particles and are tightly packed. Figure 6 shows that the model predictions are in reasonable agreement with Walton's results. The exception is the discrepancy observed in the velocity profile near the wall. Here the predicted mean velocity overestimates the simulation data. In particular, the wall slip velocity is overpredicted. This discrepancy may be attributed to the inaccuracy of the bumpy wall boundary conditions used in the model.

The present model predictions are compared with the simulation results of Campbell & Brennen (1985) for gravity flows of two-dimensional non-frictional circular disks in figures 7 and 8. The smooth boundary surface used in the simulation of Campbell & Brennen is modelled by taking the wall parameters as $\hat{s} = 0$ and $\hat{d} = 10$. The other parameters used in the present computation (which are shown on the figures) are identical to those of Campbell & Brennen. From figures 7(*a*) and 8(*a*), it is observed that the predicted non-dimensional mean velocity profiles are in good agreement with the molecular dynamics (MD) simulation results. For comparison, in figures 7(*b*) and 8(*b*) the two-dimensional solid volume fraction ν_{2D} of Camp-

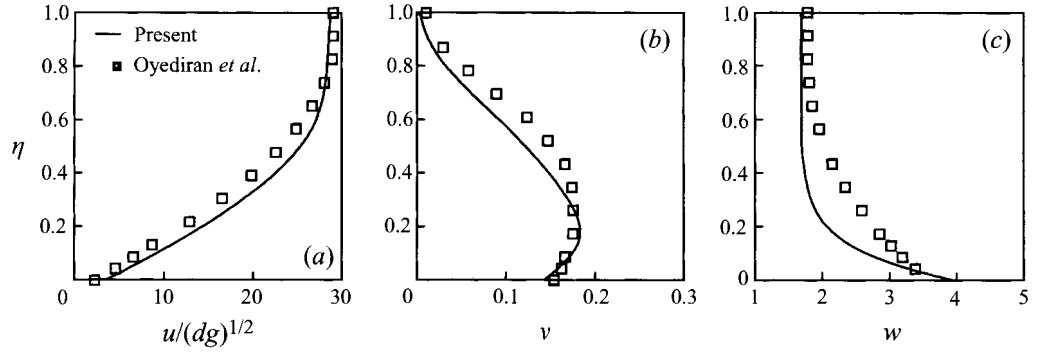

FIGURE 9. Non-dimensional (*a*) mean velocity, (*b*) solid volume fraction and (*c*) SR-fluctuation kinetic energy profiles for a gravity chute flow with $\alpha = 20.7°$, $\hat{s} = 0.414$, $\hat{d} = 0.5$, $r = 0.8$, $r_w = 0.95$, $\mu = \mu_w = 0$, $H/d = 23$. Comparison with the simulation results of Oyediran *et al.* (1994).

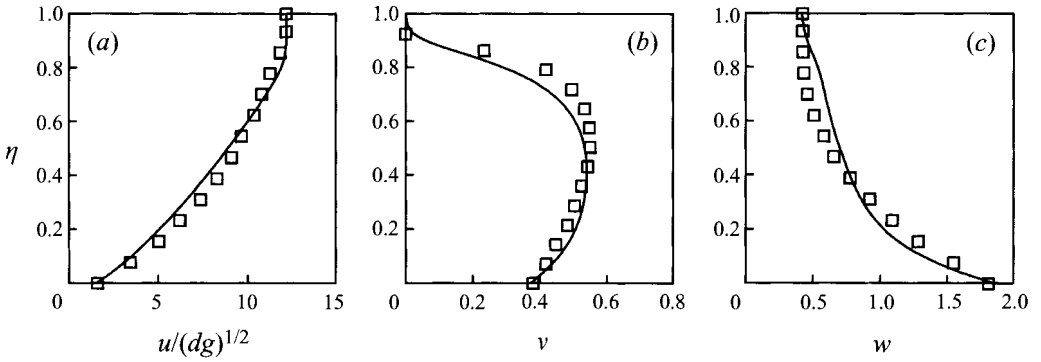

FIGURE 10. As figure 9 but for $H/d = 14$.

bell & Brennen is also converted into the equivalent three-dimensional data using $\nu_{3D} = 4\nu_{2D}^{3/2}/3\pi^{1/2}$, as was suggested by Campbell & Gong (1986). While qualitative agreement exists, the predicted solid volume fraction profiles show some deviation from the simulation results. As noted before, the model is for spherical particles, while the MD simulation of Campbell & Brennen was for circular disks, and it may have deviated somewhat from the steady-state condition. Therefore, some differences should be expected. Figures 7(*c*) and 8(*c*) show the model predictions for SR-fluctuation kinetic energy profiles. It is observed that the fluctuation energy is rather large near the boundary and decreases sharply up to about 10% of the layer height. Then it follows a slowly decreasing trend up to the free surface. Unfortunately, the corresponding MD simulation results in this case were not reported by Campbell & Brennen for comparison.

In figures 9 and 10, the present model predictions are compared with the model of Oyediran *et al.* (1994) for gravity flows of non-frictional spheres down a chute with an inclination angle of 20.7°. The bumpy wall parameters used are $\hat{s} = 0.414$ and $\hat{d} = 0.5$. The particle–particle and particle–wall restitution coefficients are taken as $r = 0.8$ and $r_w = 0.95$, the same as those used by Oyediran *et al.* (1994). Figure 9 shows the mean velocity, solid volume fraction and SR-fluctuation kinetic energy for a dilute case with an average solid volume fraction of $\bar{\nu} = 0.107$ and a granular height of $H/d = 23$. The results corresponding to a relatively dense flow with $\bar{\nu} = 0.444$

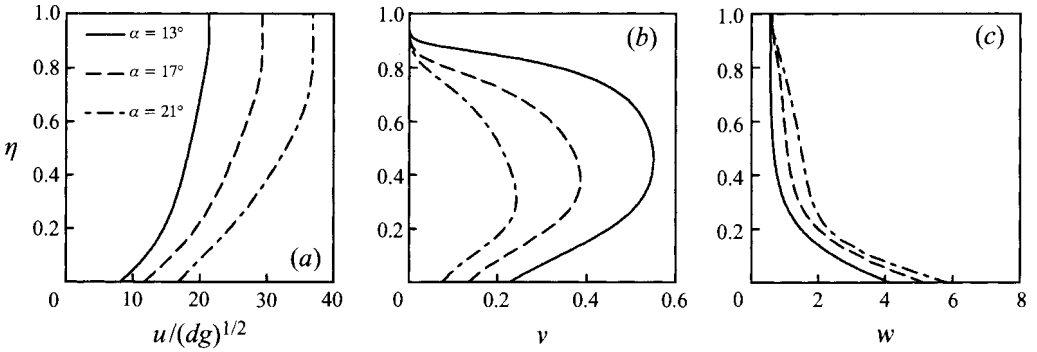

FIGURE 11. Variations of (*a*) velocity, (*b*) solid volume fraction and (*c*) SR-fluctuation kinetic energy profiles for different inclination angles for a chute flow with $\hat{s} = 0$, $\hat{d} = 1$, $H/d = 20$, $r = r_w = 0.9$, $\mu = \mu_w = 0$.

and $H/d = 14$ are shown in figure 10. These figures show that the present model predictions are in good agreement with the results of Oyediran *et al.* (1994).

Mean velocity, solid volume fraction and SR-fluctuation kinetic energy profiles of non-frictional particle chute flows are displayed in figure 11. Three different inclination angles are considered and the other parameters are kept fixed at $r = r_w = 0.9$, $\hat{s} = 0$, $\hat{d} = 1$ and $H/d = 20$. The velocity profiles shown in figure 11(*a*) indicate that a large degree of slip at the bottom wall occurs. As the inclination angle increases, the mean, as well as the slip velocities, also increase, while the solid volume fraction decreases. The flow is also very sensitive to changes of the inclination angle, since a small change in α can have a dramatic effect on the flow properties. Saltation regions with very low solid volume fraction near the free surface are also clearly observed. The height of the saltation region increases as the inclination angle increases. Figure 11(*a*) also shows that the mean velocity is roughly constant in the saltation region.

Figure 11(*b*) shows that the flow maintains a region of low density near the bottom wall. This phenomenon was observed experimentally in chute flows by Bailard (1978) and Ridgway & Rupp (1970) and in slurry flows by Shook *et al.* (1968). The molecular dynamic simulations of Campbell & Brenner (1985) and Walton (1992) and the theoretical model of Oyediran *et al.* (1994) also show similar trends of variation. The experimental data of Drake & Shreve (1986) and the corresponding model prediction shown in figure 3(*b*), however, show a peak concentration at the wall. These results indicate that the presence of a rough wall and frictional particles leads to a roughly monotonic increase of solid volume fraction toward the wall, while peak concentration for smooth wall and/or frictionless particle occurs at some distance from the wall.

Variations of the non-dimensional SR-fluctuation kinetic energy, w, are shown in figure 11(*c*). It is observed that there is a region of large fluctuation energy near the wall. This is because one main source of the fluctuation energy production is the collisions between particles and wall and the occurrence of the slip velocity. Thus, the highest fluctuation energy is found in the neighbourhood of the wall. Away from the wall, the fluctuation kinetic energy generally decreases and reaches its minimum value at the free surface. This behaviour is quite different from that for frictional particles which maintain a region of low fluctuation energy near the wall as shown in figure 3. Figure 11(*c*) also shows that as the inclination angle of the chute increases, the fluctuation kinetic energy increases.

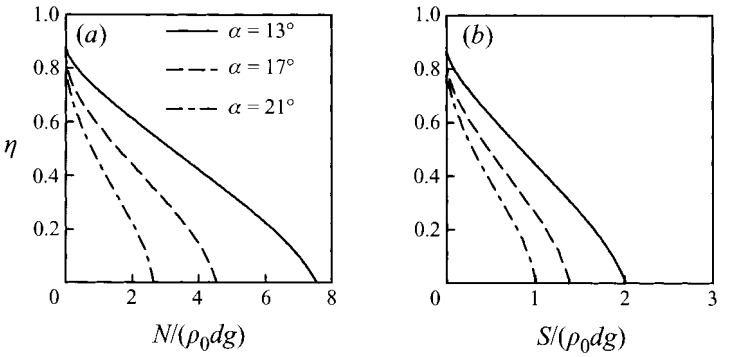

FIGURE 12. Variations of (*a*) non-dimensional normal and (*b*) tangential stresses for different inclination angles for a chute flow with $\hat{s} = 0$, $\hat{d} = 1$, $H/d = 20$, $r = r_w = 0.9$, $\mu = \mu_w = 0$.

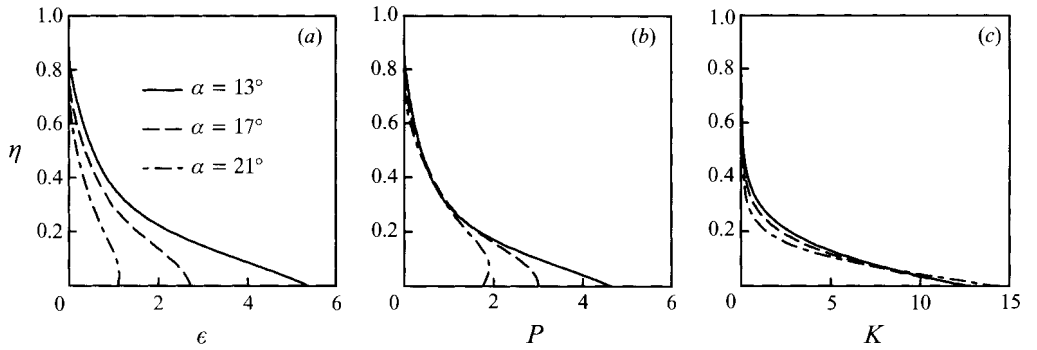

FIGURE 13. Variations of (*a*) non-dimensional energy dissipation, (*b*) energy production and (*c*) fluctuation energy flux for different inclination angles for a chute flow with $\hat{s} = 0$, $\hat{d} = 1$, $H/d = 20$, $r = r_w = 0.9$, $\mu = \mu_w = 0$.

For the conditions of figure 11, the variations of non-dimensional normal stress, $\hat{N} = N/(\rho_0 dg)$, tangential stress, $\hat{S} = S/(\rho_0 dg)$, energy dissipation, $\hat{\epsilon} = \rho\epsilon/[\rho_0(dg)^{3/2}/d]$, energy production, $\hat{P} = \hat{S}\mathrm{d}\hat{u}/\mathrm{d}\eta$, and fluctuation energy flux, $\hat{K} = K_2/[\rho_0(dg)^{3/2}]$, are shown in figures 12 and 13. Figure 12 shows that the normal and tangential stresses have their highest values at the wall, and their magnitudes decrease with increasing distance from the wall. As the inclination angle increases, the non-dimensional normal and tangential stresses decrease. Figure 13 shows that the energy production, the energy dissipation and the fluctuation energy flux, generally, increase toward the wall. It is also observed that the energy dissipation and production rates decrease as α increases, while the fluctuation energy flux increases very near the wall and decreases at distances away from the wall. Figures 12 and 13 show that the normal and tangential stresses, the energy production and disspation rates and the fluctuation energy flux are very small in the saltation region.

The effects of frictional energy losses on chute flows are studied and the results for different wall–particle spacings are presented in figures 14 and 15. Here μ is varied, while the other parameters are kept fixed at H/d=16, $\alpha = 42.75°$, $\hat{d} = 1$ and $r = r_w = 0.84$. Figures 14(*a*) and 15(*a*) shows variations of the mean velocity profile with height for different friction coefficients. It is observed that the slip velocity decreases when the friction coefficient increases. The amount of decrease of slip velocity with μ is significantly enhanced as wall roughness ($\hat{s}$) increases.

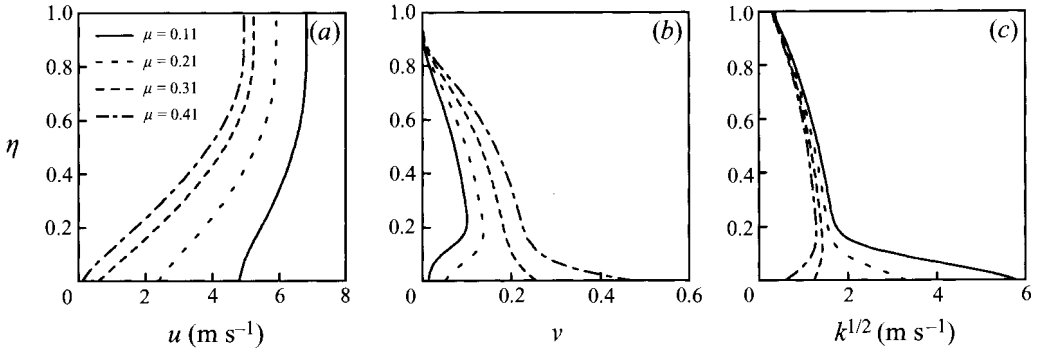

FIGURE 14. Variations of (*a*) mean velocity, (*b*) solid volume fraction and (*c*) SR-fluctuation kinetic energy profiles for different friction coefficients for a gravity flow with $\alpha = 42.75°$, $r_w = r = 0.84$, $\mu_w = \mu$, $\hat{s} = 0$, $\hat{d} = 1$, $H/d = 16$.

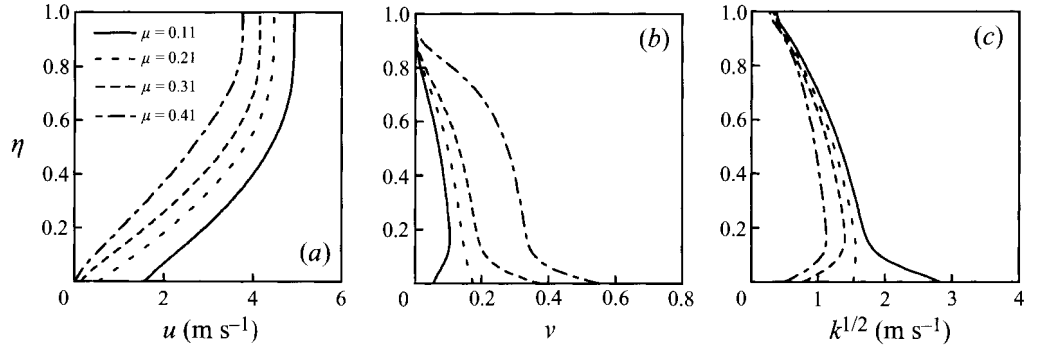

FIGURE 15. As figure 14 but for $\hat{s} = 0.4$

Figures 14(*b*) and 15(*b*) indicate that as μ increases, the solid volume fraction increases. For a low value of friction coefficient, the flow has a region of low solid volume fraction near the wall, and ν increases with distance from the wall to a certain maximum. It then decreases and becomes quite small in the saltation region. For a high value of friction coefficient, however, the solid volume fraction decreases monotonically with distance from the bed. As noted before, both increasing and decreasing trends of variation of ν with distance from the bed were observed experimentally. The present results suggest that the combination of frictional loss of energy and wall roughness controls the resulting behaviour. Based on figures 14 and 15, there appears to be a specific range of friction coefficients for which the transition between these two flow patterns occurs. The transition friction coefficient varies with the wall roughness. For $\hat{s} = 0.4$, figure 15(*b*) shows that the transition friction coefficient is about 0.2, while figure 14(*b*) (for $\hat{s} = 0$) indicates that the transition occurs for μ close to 0.3.

The fluctuation kinetic energy variations with μ and $\hat{s}$ are shown in figures 14(*c*) and 15(*c*). These figures show that as μ increases, the fluctuation kinetic energy decreases. A change in friction coefficient strongly affects the fluctuation energy profile near the wall. The trend of variation, however, is opposite to that observed for ν. For a small friction coefficient, k is rather large near the wall and decreases sharply with distance from the wall up to about 20% of the height and then decreases gradually toward the free surface. For a high value of friction coefficient, however, fluctuation energy is

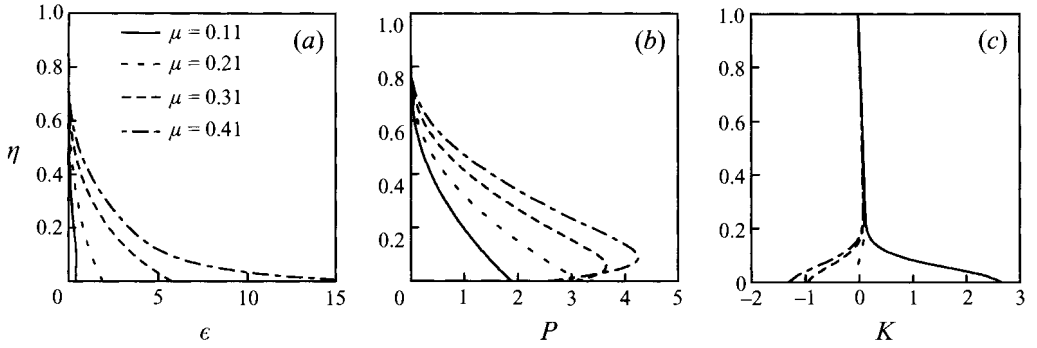

FIGURE 16. Variations of (*a*) non-dimensional energy dissipation, (*b*) energy production and (*c*) fluctuation energy flux for different friction coefficients for a gravity flow with $\alpha = 42.75°$, $r_w = r = 0.84$, $\mu_w = \mu$, $\hat{s} = 0.4$, $\hat{d} = 1$, $H/d = 16$.

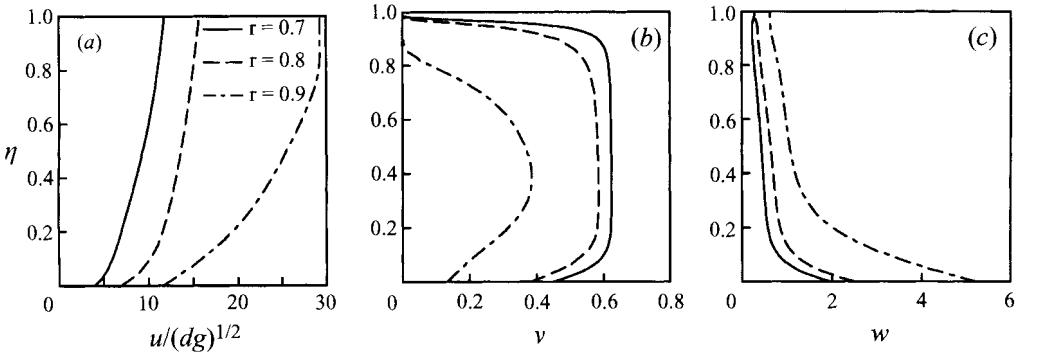

FIGURE 17. Effects of particle–particle restitution coefficient r on (*a*) mean velocity, (*b*) solid volume fraction and (*c*) SR-fluctuation kinetic energy profiles for a bumpy chute with $\alpha = 17°$, $\hat{s} = 0$, $\hat{d} = 1$, $r_w = 0.9$, $\mu = \mu_w = 0$, $H/d = 20$.

low near the wall and increases with distance from the wall to a maximum and then decreases gradually toward to the free surface.

For frictional granules, the non-dimensional energy dissipation, energy production and fluctuation energy flux are shown in figure 16. The friction coefficient $\mu = \mu_w$ is varied, while the other parameters which are listed in the figure caption are kept fixed. It is observed that the energy dissipation decreases with the distance from the wall. Furthermore, both dissipation and production increase as friction coefficient increases, with $\hat{\epsilon}$ increasing at much faster rate. For a small friction coefficient, the maximum energy production occurs at the wall, and $\hat{P}$ decreases with distance from the wall. For a relatively large friction coefficient, however, the peak energy production occurs at some distances from the wall. Near the wall region, figure 16(*c*) shows that the energy flux switches sign at certain value of (transition) friction coefficient. Here for $\mu < 0.21$, $\hat{K}$ is positive indicating that the production of energy near the wall exceeds the dissipation rate. Thus, fluctuation energy flows from the wall toward the free surface. For $\mu > 0.21$, however, $\hat{K}$ is negative near the wall. This implies that $\hat{P}$ is larger than $\hat{\epsilon}$ at some distance away from the wall and fluctuation energy diffuses toward the wall. These observations are consistent with the trend of variation of fluctuation energy profiles shown in figure 15(*c*).

Typical results for different values of coefficient of restitution, r, are shown in figure 17. The parameters used in the numerical calculation are listed in the figure caption.

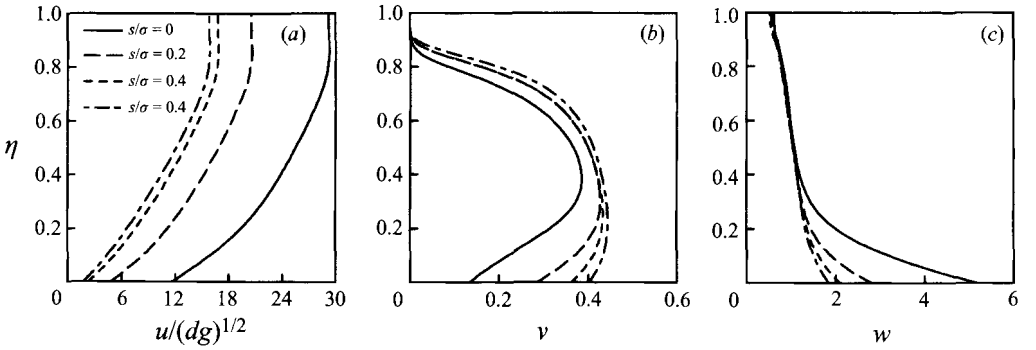

FIGURE 18. Variations of (*a*) velocity, (*b*) solid volume fraction and (*c*) SR-fluctuation kinetic energy profiles for different roughness parameter $\hat{s}$ (s/σ) for a chute flow with $\hat{d} = 1$, $r = r_w = 0.9$, $\mu_w = \mu = 0$, $H/d = 20$, $\alpha = 17°$.

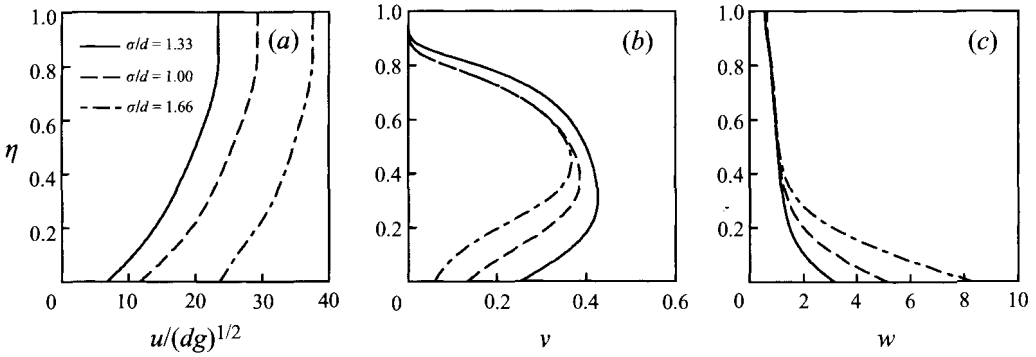

FIGURE 19. As figure 18 but for different roughness parameter σ/d ($\hat{d}^{-1}$).

It is observed that higher values of restitution coefficient r tend to increase the mean velocity and the corresponding slip at wall, as well as the fluctuation kinetic energy. The solid volume fraction, however, decreases as the particles become more elastic. It is also observed that the velocity, solid volume fraction and fluctuation kinetic energy are more sensitive to the variation of r as the restitution coefficient becomes closer to one.

As noted in §3, the wall roughness can be adjusted by changing parameters $\hat{s}$ or $\hat{d}$. The variations of mean velocity, solid volume fraction and SR-fluctuation kinetic energy with wall roughness parameters are shown in figures 18 and 19. The other parameters used in the simulation are listed in the figure captions. When $\hat{s}$ increases or $\hat{d}$ decreases, the boundary becomes more rough, and both the mean and the slip velocities decrease. However, the heights of the saltation region remain nearly unchanged. From figures 18(*b*) and 19(*b*), it is observed that the solid volume fraction increases and the SR-fluctuation kinetic energy decreases as $\hat{s}$ increases or $\hat{d}$ decreases. Figures 18(*c*) and 19(*c*) show that the fluctuation kinetic energy remains nearly unchanged at some distance away from the wall.

7. Conclusions

A kinetic model that includes the frictional energy losses and the extended kinetic-based boundary condition was used to numerically study gravity granular flows down

an inclined bumpy chute. Based on the presented results, the following conclusions may be drawn:

(i) Steady granular gravity flow could be achieved at an arbitrary inclination angle for rough bumpy frictional chutes.

(ii) The present computational model is capable of predicating the features of gravity-driven rapid granular flow, and the model predictions are in good agreement with the available experimental data and digital simulation results.

(iii) The velocity profiles of gravity granular flow down an inclined bumpy chute generally consist of two parts, a roughly parabolic region with a significant slip at the wall and a saltation region with nearly constant velocity.

(iv) For rapid granular gravity flows of frictionless particles in the collision-dominant (grain-inertia) regime over a smooth incline, the solid volume fraction remains somewhat low near the wall, increases to a maximum at some distance from the wall, and then decreases gradually to zero at the free surface. For highly frictional particles and rough walls, the solid volume fraction increases monotonically with depth, and its peak value occurs at the wall. These trends of variation are well predicted by the present model.

(v) In the saltation region near the diffused free surface, the solid volume fraction is very low.

(vi) At the wall, there is a large rate of generation of fluctuation kinetic energy due to the occurrence of slip velocity and a region of high velocity gradient. As a result, the fluctuation kinetic energy is quite high near the wall. For frictionless granules and smooth walls, the peak fluctuation energy and its maximum production rate occur at the wall. For frictional particles and rough walls, these peaks move to some short distances away from the wall.

(vii) The flow is quite sensitive to variation of the inclination angle. As the inclination angle increases, the mean velocity and the corresponding slip increase rapidly, while the solid volume fraction decreases.

(viii) The flow depth has a significant effect on the behaviour of granular flow. As the flow depth increases, the velocity and the slip velocity decrease, while the solid volume fraction and the fluctuation kinetic energy increase.

(ix) Effects of frictional energy losses during particle–particle and particle–wall collisions are important. As friction coefficient increases, the height of the saltation region and the slip velocity decrease, and the solid volume fraction profile becomes more flat.

(x) The combination of frictional energy loss and wall roughness strongly affects the trends of variation of solid volume fraction and fluctuation energy profiles in granular gravity flows. A small friction coefficient and a smooth wall lead to a region of low density and high fluctuation energy in the neighbourhood of the wall. For high friction coefficients and rough walls, the solid volume fraction increases monotonically up to the wall, while a region of low fluctuation energy is formed near the solid surface.

(xi) As the restitution coefficient r increases, the velocity and the slip velocity, as well as the fluctuation kinetic energy, increase, while the solid volume fraction decreases.

(xii) The surface roughness significantly affects the velocity, solid volume fraction and fluctuation kinetic energy profiles. As s/σ decreases or σ/d increases, the mean velocity, the slip velocity and the fluctuation kinetic energy decrease, while the solid volume fraction increases.

The authors would like to thank Professor Richman for making his paper with Oyediran, Martin and Alexandrou (1994) available to them prior to publication. This work was supported by the US Department of Energy (University Coal Research Program, PETC) under Grants DE-FG-22-91PC91297 and DE-FG-94PC94213. GA also would like to thank the National Research Council and the Morgantown Energy Technology Center for their support during the later stages of this work.

Appendix A. Order of rotational fluctuation energy

The purpose of this Appendix is to evaluate the order of rotational fluctuation kinetic energy relative to the translational one.

Suppose particle A with a velocity v_1 and spin ω_1 collides with a fixed particle B. (For simplicity, it is assumed that particle B is fixed, but the results also apply when particle B is moving.) Let v_2 and ω_2 denote the velocity and spin of particle A after the collision. Balance of momentum and angular momentum during collision implies that

$$\int_{\Delta t} N \mathrm{d}t \sim m(v_2 - v_1) = mv', \tag{A 1}$$

$$d \int_{\Delta t} T \mathrm{d}t \sim I(\omega_2 - \omega_1) = I\omega', \tag{A 2}$$

where m and d are mass and diameter of particle, A, N and T are the normal and tangential forces acting on the particle, $I = \frac{1}{10}md^2$ is the moment of inertia, and Δt is the time duration of collision. Here v' and ω' are the order of the particle fluctuation velocity and spin. The normal and tangential forces are related by

$$T \leqslant \mu N, \tag{A 3}$$

where μ is the contact frictional coefficient.

Using (A1) and (A3), equation (A2) may be restated as

$$I\omega' \sim \mu m v' d, \tag{A 4}$$

or

$$\omega' \sim \mu \frac{v'}{d}. \tag{A 5}$$

Therefore, the ratio of the rotational fluctuation kinetic energy to the translational fluctuation kinetic energy is given as

$$\frac{I\omega'^2}{mv'^2} \sim \frac{d^2\omega'^2}{v'^2} \sim \mu^2. \tag{A 6}$$

Thus the ratio of rotational fluctuation kinetic energy to the translational one is of the order of μ^2, and becomes negligible for a small frictional coefficient.

Appendix B. Boundary conditions for a slightly frictional bumpy wall

In this Appendix, the boundary conditions for a bumpy wall and granules with small inelasticity and friction are derived. The expressions for the rate of momentum supply to the granular flow, $\boldsymbol{M}$, and the rate of energy dissipation D due to boundary–flow collisions per unit area are also evaluated. The geometry of the bumpy boundary is shown in figure 1, and it is assumed that the wall is moving with a velocity $\boldsymbol{U}$.

The velocity c' of the centre of a flow particle immediately after the collision is related to its velocity c immediately before the collision through

$$c' = c + \frac{1}{m}\int_{\Delta t} F \mathrm{d}t, \tag{B 1}$$

where F is the impact force, Δt is the duration of collision and m is the mass of the flow particle. For nearly elastic particles and a small coefficient of friction, μ_w, the impulse per unit mass is given as (e.g. Ahmadi & Shahinpoor 1983)

$$\frac{1}{m}\int_{\Delta t} F \mathrm{d}t = (1 + r_w)(g \cdot k)(k + \mu_w t), \tag{B 2}$$

where r_w is the coefficient of restitution, k is the unit vector directed from the centre of the wall sphere toward the centre of the flow particle, t is the unit tangent to the spheres in the plane of g and k, and $g = U - c$ is the relative velocity of the particle centres just before the collision. Since t is also perpendular to k, it follows that

$$t = \frac{k \times (g \times k)}{|k \times (g \times k)|}. \tag{B 3}$$

In the derivation of (B2), it was assumed that the frictional slip occurs during the collisions, and the rotational effects are negligible for small friction coefficients and small granules as described in Appendix A. Using (B2), equation (B1) may be restated as

$$c' = c + (1 + r_w)(g \cdot k)(k + \mu_w t). \tag{B 4}$$

Therefore,

$$c'^2 \approx c^2 + 2(1 + r_w)(g \cdot k)[U \cdot (k + \mu_w t)] - (1 - r_w^2)(g \cdot k)^2 - 2\mu_w(1 + r_w)(g \cdot k)(g \cdot t), \tag{B 5}$$

where the μ_w^2 term is neglected.

Let $f(c, r, t)$ be the velocity distribution function at position r and velocity c and $\psi = \psi(c)$ be a property associated with a flow particle, and $\Delta\psi = \psi(c') - \psi(c)$ denotes its change due to a collision with a wall particle. Then, according to Jenkins & Richman (1985) and Richman (1988), for unit area of the wall the rate of change of $\psi(c)$ in collisions, $\mathbb{C}$, is given by

$$\mathbb{C}(\psi) = \frac{m\omega \operatorname{cosec}^2\theta}{\pi}\iint \Delta\psi f(c, r + \sigma_0 k)(g \cdot k)\mathrm{d}\bar{k}\mathrm{d}c, \tag{B 6}$$

where $\sigma_0 = (d + \sigma)/2$ is the distance from the centre of the wall particle to the centre of the flow particle. The integrations are to be taken over all angles $\bar{k}$, $-\theta \leqslant \bar{k} \leqslant 0$, and velocities c for which a collision is impending, $g \cdot k \geqslant 0$.

When $\psi = mc$, according to (B4) $\Delta\psi = m(c' - c) = m(1 + r_w)(g \cdot k)(k + \mu_w t)$, and the collisional rate of supply of momentum M to the flow per unit area of the wall is given as

$$M = M^r + M^f. \tag{B 7}$$

with

$$M^r = \frac{m\omega \operatorname{cosec}^2\theta}{\pi}(1 + r_w)\iint k f(c, r + \sigma_0 k)(g \cdot k)^2 \mathrm{d}\bar{k}\mathrm{d}c, \tag{B 8}$$

$$M^f = \frac{\mu_w m\omega \operatorname{cosec}^2\theta}{\pi}(1 + r_w)\iint t f(c, r + \sigma_0 k)(g \cdot k)^2 \mathrm{d}\bar{k}\mathrm{d}c. \tag{B 9}$$

Here the superscripts r and f, respectively, refer to the restitution (inelasticity) and the frictional effects.

When $\psi \doteq \frac{1}{2}mc^2$, and $\Delta\psi = \frac{1}{2}m(c'^2 - c^2)$, using (B5), the collisional rate of supply of energy E to the flow per unit area of the wall is given as

$$E = \boldsymbol{M} \cdot \boldsymbol{U} - D. \tag{B 10}$$

Here the expression for the energy loss, D, may also be decomposed as

$$D = D^r + D^f, \tag{B 11}$$

where

$$D^r = \frac{m\omega(1+r_w)\mathrm{cosec}^2\theta}{2\pi} \int\int (1-r_w) f(\boldsymbol{c}, \boldsymbol{r}+\sigma_0\boldsymbol{k})(\boldsymbol{g}\cdot\boldsymbol{k})^3 \mathrm{d}\bar{k}\mathrm{d}\boldsymbol{c}, \tag{B 12}$$

$$D^f = \frac{m\omega(1+r_w)\mathrm{cosec}^2\theta}{2\pi} \int\int 2\mu_w f(\boldsymbol{c}, \boldsymbol{r}+\sigma_0\boldsymbol{k})(\boldsymbol{g}\cdot\boldsymbol{k})^2(\boldsymbol{g}\cdot\boldsymbol{t})\mathrm{d}\bar{k}\mathrm{d}\boldsymbol{c}. \tag{B 13}$$

Note that in equation (B13), only the terms up to the first order in μ_w are retained.

For non-frictional nearly elastic particles with a diameter d, using the the distribution function,

$$f(\boldsymbol{c}, \boldsymbol{r}, t) = n(2\pi T)^{-3/2}[1 - (\sqrt{2}dB/\pi^{1/2}T^{3/2}\boldsymbol{C}\cdot\hat{\boldsymbol{D}}\cdot\boldsymbol{C}]\exp(-C^2/2T), \tag{B 14}$$

Richman (1988) has shown that $\boldsymbol{M}_i^r$, up to an error of order ϵ, and D^r, up to an error of order $\epsilon^{3/2}$, have the following forms:

$$\boldsymbol{M}_i^r = \tfrac{1}{2}(1+r_w)\rho\omega T \left\{ \lambda_i + (2/\pi)^{1/2}(2v_i/3T^{1/2})[2\mathrm{cosec}^2\theta(1-\cos\theta) - \cos\theta] + (2/\pi)^{1/2}\left(\sigma_0 \frac{\partial u_k}{\partial x_j}\left[\left(1+B\frac{d}{\sigma_0}\right)I_{ijk} + \lambda_j I_{ik}\right]\right)\right\} \tag{B 15}$$

$$D^r = (2/\pi)^{1/2}(1-r_w)\rho\omega(1+r_w)T^{3/2}(1-\cos\theta)\mathrm{cosec}^2\theta, \tag{B 16}$$

where $\epsilon \equiv \sigma_0/L$ is a small quantity. Here L is a characteristic length of the mean field (Jenkins & Richman 1986). Therefore, only the frictional contributions, $\boldsymbol{M}^f$ and D^f, need to be evaluated.

Let

$$\boldsymbol{g} = g_1\boldsymbol{k} + g_2\boldsymbol{l} + g_3\boldsymbol{m}, \tag{B 17}$$

where $\boldsymbol{l}$, $\boldsymbol{m}$ and $\boldsymbol{k}$ are unit orthogonal vectors. Equation (B3) then implies

$$\boldsymbol{t} = \frac{1}{(g_2^2+g_3^2)^{1/2}}(g_2\boldsymbol{l} + g_3\boldsymbol{m}). \tag{B 18}$$

Assuming that μ_w is of order $\epsilon^{1/2}$ and expanding $f(\boldsymbol{c}, \boldsymbol{r}+\sigma_0\boldsymbol{k})$ in terms of ϵ, equation (B9) up to an error of order ϵ becomes

$$\boldsymbol{M}^f = \frac{\mu_w\omega\,\mathrm{cosec}^2\theta}{\pi}\frac{(1+r_w)mn}{(2T)^{3/2}} \int\left\{\int_0^\infty g_1^2 \mathrm{e}^{-g_1^2/2T}\mathrm{d}g_1 \left[\boldsymbol{l}\int_{-\infty}^\infty \mathrm{e}^{-g_3^2/2T}\left(\int_{-\infty}^\infty \frac{g_2\mathrm{e}^{-g_2^2/2T}}{(g_2^2+g_3^2)^{1/2}}\mathrm{d}g_2\right)\mathrm{d}g_3 + \boldsymbol{m}\int_{-\infty}^\infty \mathrm{e}^{-g_2^2/2T}\left(\int_{-\infty}^\infty \frac{g_3\mathrm{e}^{-g_3^2/2T}}{(g_2^2+g_3^2)^{1/2}}\mathrm{d}g_3\right)\mathrm{d}g_2\right]\right\}\mathrm{d}\bar{k}, \tag{B 19}$$

Noting that the terms in large parentheses in equation (B19) are zero, it follows that

$$\boldsymbol{M}^f = 0. \tag{B 20}$$

Similarly, up to order ϵ, D^f as given by equation (B13) becomes

$$D^f = \frac{\mu_w mn\omega(1+r_w)\mathrm{cosec}^2\theta}{\pi(2\pi T)^{3/2}} \int_0^\infty \int_0^\infty g_1^2 e^{-g_1^2/2T} dg_1 \int_{-\infty}^\infty \int_{-\infty}^\infty (g_2^2+g_3^2)^{1/2} e^{-(g_2^2+g_3^2)/2T} dg_2 dg_3 d\bar{k} \tag{B 21}$$

or

$$D^f = (2/\pi)^{1/2}(\tfrac{1}{2}\pi\mu_w)\rho\omega(1+r_w)T^{3/2}(1-\cos\theta)\mathrm{cosec}^2\theta. \tag{B 22}$$

Note that $\int d\bar{k} = 2\pi(1-\cos\theta)$ and $\rho = mn$ are used in the derivation of equation (B21).

Using (B20) and (B22) in equations (B7) and (B11), it follows that for frictional particles with a small frictional coefficient μ_w (of order $\epsilon^{1/2}$), $\boldsymbol{M}_i$, is given as

$$\boldsymbol{M}_i = \tfrac{1}{2}(1+r_w)\rho\omega T \left\{ \lambda_i + (2/\pi)^{1/2}(2v_i/3T^{1/2})[2\mathrm{cosec}^2\theta(1-\cos\theta) - \cos\theta] + (2/\pi)^{1/2} \left(\sigma_0 \frac{\partial u_k}{\partial x_j} \left[\left(1 + B\frac{d}{\sigma_0} \right) I_{ijk} + \lambda_j I_{ik} \right] \right\}, \tag{B 23}$$

and D is given by

$$D = (2/\pi)^{1/2}(1 - r_w + \tfrac{1}{2}\pi\mu_w)\rho\omega(1+r_w)T^{3/2}(1-\cos\theta)\mathrm{cosec}^2\theta. \tag{B 24}$$

Now restating the granular temperature $T(=\frac{2}{3}k)$ in terms of the fluctuation kinetic energy k, and using $1 + r_w \approx 2$ for nearly elastic particles, equations (B23) and (B24) are reduced to equations (15) and (16), when the factor of $\pi/4$ is approximated as unity.

REFERENCES

Abu-Zaid, S. & Ahmadi, G. 1990 Simple kinetic model for rapid granular flows including frictional losses. *J. Engng Mech. ASCE* **116**, 379–389.

Abu-Zaid, S. & Ahmadi, G. 1993 Analysis of rapid shear flows of granular materials by a kinetic model including frictional losses. *Powder Technol.* **77**, 7–17.

Ahmadi, G. & Ma, D. 1986 A Kinetic model for granular flows of nearly elastic particles in grain-inertia regime. *Intl J. Bulk Solids Storage in Silos* **2**, 8–16.

Anderson, K. G. & Jackson, R. 1992 A comparison of the solutions of some proposed equations of motion of granular materials for fully developed flow down inclined planes. *J. Fluid Mech.* **241**, 145–168.

Augenstein, D. A. & Hogg, R. 1978 An experimental study of dry powders on inclined surfaces. *Powder Technol.* **19**, 205–215.

Bailard, J. 1978 An experimental study of granular-fluid flow. PhD Dissertation, Univ. Calif., San Diego, La Jolla.

Campbell, C. S. & Brennen, C. E. 1985 Chute flows of granular material: some numerical simulations. *Trans. ASME J. Appl. Mech.* **172**, 172–178.

Campbell, C. S., Brennen, C. E. & Sabersky, R. H. 1985 Flow regimes in inclined open-channel flows of granular materials. *Powder Technol.* **41**, 77–82.

Campbell, C. S. & Gong, A. 1986 The stress tensor in a two-dimensional granular shear flow. *J. Fluid Mech.* **164**, 107–125.

Cao, J. & Ahmadi, G. 1995 Numerical simulation of frictional granular Couette flows between two bumpy parallel plates. *Particulate Sci. Tech.* **13**, 133–147.

Drake, T. G. 1990 Structural features in granular flows. *J. Geophys. Res.* **95**, 8681–8696.

Drake, T. G. 1991 Granular flow: physical experiments and their implications for microstructural theories. *J. Fluid Mech.* **225**, 121–152.

DRAKE, T. G. & SHREVE, R. L. 1986 High-speed motion pictures of nearly steady, uniform, two-dimensional, inertial flows of granular material. *J. Rheol.* **50**, 981–993.

GUDHE, R., RAJAGOPAL, K. R. & MASSOUDI, M. 1994 Fully developed flow of granular materials down a heated inclined plane. *Acta Mechanica* **103**, 63–78.

HANES, D. M., JENKINS, J. T. & RICHMAN, M. W. 1988 The thickness of steady plane shear flows of circular disks driven by identical boundaries. *Trans. ASME J. Appl. Mech.* **55**, 969–974.

HUI, K., HAFF, P. K., UNGAR, J. E. & JACKSON, R. 1984 Boundary conditions for high shear grain flows. *J. Fluid Mech.* **145**, 223–233.

JENKINS, J. T. 1992 Boundary conditions for rapid granular flow: flat, frictional walls. *Trans. ASME J. Appl. Mech.* **59**, 120–127.

JENKINS, J. T. & HANES, D. M. 1993 The balance of momentum and energy at an interface between colliding and freely flying grains in a rapid granular flow. *Phys. Fluids* A **5**, 781–783.

JENKINS, J. T. & RICHMAN, M. W. 1985 Grad's 13-moment systems for a dense gas of inelastic spheres. *Arch. Rat. Mech. Anal.* **87**, 355–377.

JOHNSON, P. C., NOTT, P. & JACKSON, R. 1990 Frictional-collisional equations of motion for particulate flows and their application to chutes. *J. Fluid Mech.* **210**, 501–535.

LUN, C. K. K. & SAVAGE, S. B. 1987 A simple kinetic theory for granular flow of rough, inelastic, spherical particles. *Trans. ASME J. Appl. Mech.* **54**, 47–53.

OYEDIRAN, A. A., RICHMAN, M. W., MARTIN, R. E. & ALEXANDROU, A. N. 1994 Granular flows down bumpy inclines: numerical solutions. *Acta Mechanica* (in press).

PASQUARELL, G. C., ACKERMANN, N. L., SHEN, H. H. & HOPKINS, M. A. 1988 Collisional stress in granular flows, bagnold revisited. *J. Engng Mech. ASCE* **114**, 49–64.

PATTON, J. S., BRENNEN, C. E. & SABERSKY, R. H. 1987 Shear flows of rapidly flowing granular materials. *Trans. ASME J. Appl. Mech.* **54**, 801–805.

RICHMAN, M. W. 1988 Boundary conditions based upon a modified Maxwellian velocity distribution for flow of identical, smooth, nearly elastic spherical. *Acta Mechanica* **75**, 227–240.

RICHMAN, M. W. & MARCINIEC, R. P. 1990 Gravity-driven granular flows of smooth, inelastic spheres down bumpy inclines. *Trans. ASME J. Appl. Mech.* **57**, 1036–1043.

RIDGWAY, K. & RUPP, R. 1970 Flows of granular material down chutes. *Chem. Process Engng* **51**, 82–85.

SAVAGE, S. B. 1978 Experiments on shear flows of cohesionless granular material. In *Proc. US-Japan Seminar on Continuum-Mechanical and Statistical Approaches in the Mechanics of Granular Material*, pp. 241-254. Gakujutsu Bunken Fukyukai. Tokyo.

SAVAGE, S. B. 1979 Gravity flows cohesionless granular materials in chutes and channels. *J. Fluid Mech.* **92**, 53–96.

SAVAGE, S. B. & DAI, R. 1991 Some aspects of bounded and unbounded shear flows of granular materials. In *Micromechanics of Granular Materials, US-Japan Seminar*. Potsdam, New York.

SHOOK, C. A., DANIEL, S. M., SCOTT, J. A. & HOLGATE, J. P. 1968 Flow of suspensions in pipelines part II: mechanisms of particle suspension. *Can. J. Chem. Engng* **46**, 238–244.

WALTON, O. R. 1992 Numerical simulation of inclined chute flows of monodisperse, inelastic, frictional spheres. In *Advances in Micromechanics of Granular Materials* (ed. H. H. Shen *et al.*), pp. 453–461. Elsevier.

WALTON, O. R., BRAUN, R. L., MALLON, R. G. & CERVELLI, D. M. 1988 Particle-dynamics calculations of gravity flow of inelastic frictional spheres. In *Micromechanics of Granular Materials* (ed. M. Satake & J. T. Jenkins), pp. 152–162. Elsevier.